NeuroImage 118 (2015) 199–208

Contents lists available at ScienceDirect

NeuroImage

journal homepage: www.elsevier.com/locate/ynimg

First-in-human PET quantification study of cerebral α4β2* nicotinic acetylcholine receptors using the novel specific radioligand (−)-[^{18}F]Flubatine☆

Osama Sabri [a,b,*,1], Georg-Alexander Becker [a,1], Philipp M. Meyer [a], Swen Hesse [a,b], Stephan Wilke [a], Susanne Graef [c,d], Marianne Patt [a], Julia Luthardt [a], Gudrun Wagenknecht [e], Alexander Hoepping [f], René Smits [f], Annegret Franke [g], Bernhard Sattler [a], Bernd Habermann [a], Petra Neuhaus [g], Steffen Fischer [h], Solveig Tiepolt [a], Winnie Deuther-Conrad [h], Henryk Barthel [a], Peter Schönknecht [c,1], Peter Brust [h,1]

[a] Department of Nuclear Medicine, University of Leipzig, Liebigstraße 18, 04103 Leipzig, Germany
[b] Integrated Research and Treatment Centre (IFB) Adiposity Diseases, University of Leipzig, Philipp-Rosenthal-Straße 27, 04103 Leipzig, Germany
[c] Department of Psychiatry, University of Leipzig, Semmelweisstraße 10, 04103 Leipzig, Germany
[d] Max-Planck-Institute for Human Cognitive and Brain Sciences, Stephanstraße 1a, 04103 Leipzig, Germany
[e] Electronic Systems (ZEA-2), Central Institute for Engineering, Electronics and Analytics, Research Centre Juelich, Wilhelm-Johnen-Straße, 52428 Juelich, Germany
[f] ABX Advanced Biochemical Compounds GmbH, Heinrich-Gläser-Straße 10, 01454 Radeberg, Germany
[g] Clinical Trial Centre Leipzig, Härtelstraße 16–18, 04107 Leipzig, Germany
[h] Helmholtz-Zentrum Dresden-Rossendorf, Research Site Leipzig, Permoserstraße 15, 04318 Leipzig, Germany

ARTICLE INFO

Article history:
Received 2 October 2014
Accepted 24 May 2015
Available online 30 May 2015

Keywords:
(−)-[^{18}F]Flubatine [(−)-[^{18}F]NCFHEB]
PET
α4β2* nicotinic acetylcholine receptors
Human brain
Kinetic modeling

ABSTRACT

α4β2* nicotinic receptors (α4β2* nAChRs) could provide a biomarker in neuropsychiatric disorders (e.g., Alzheimer's and Parkinson's diseases, depressive disorders, and nicotine addiction). However, there is a lack of α4β2* nAChR specific PET radioligands with kinetics fast enough to enable quantification of nAChR within a reasonable time frame. Following on from promising preclinical results, the aim of the present study was to evaluate for the first time in humans the novel PET radioligand (−)-[^{18}F]Flubatine, formerly known as (−)-[^{18}F]NCFHEB, as a tool for α4β2* nAChR imaging and in vivo quantification.

Dynamic PET emission recordings lasting 270 min were acquired on an ECAT EXACT HR+ scanner in 12 healthy male non-smoking subjects (71.0 ± 5.0 years) following the intravenous injection of 353.7 ± 9.4 MBq of (−)-[^{18}F]Flubatine. Individual magnetic resonance imaging (MRI) was performed for co-registration. PET frames were motion-corrected, before the kinetics in 29 brain regions were characterized using 1- and 2-tissue compartment models (1TCM, 2TCM). Given the low amounts of metabolite present in plasma, we tested arterial input functions with and without metabolite corrections. In addition, pixel-based graphical analysis (Logan plot) was used. The model's goodness of fit, with and without metabolite correction was assessed by Akaike's information criterion. Model parameters of interest were the total distribution volume V_T (mL/cm^3), and the binding potential BP_{ND} relative to the corpus callosum, which served as a reference region.

The tracer proved to have high stability in vivo, with 90% of the plasma radioactivity remaining as untransformed parent compound at 90 min, fast brain kinetics with rapid uptake and equilibration between free and receptor-bound tracer. Adequate fits of brain TACs were obtained with the 1TCM. V_T could be reliably estimated within 90 min for all regions investigated, and within 30 min for low-binding regions such as the cerebral cortex.

The rank order of V_T by region corresponded well with the known distribution of α4β2* receptors (V_T [thalamus] 27.4 ± 3.8, V_T [putamen] 12.7 ± 0.9, V_T [frontal cortex] 10.0 ± 0.8, and V_T [corpus callosum] 6.3 ± 0.8). The BP_{ND}, which is a parameter of α4β2* nAChR availability, was 3.41 ± 0.79 for the thalamus, 1.04 ± 0.25 for the putamen and 0.61 ± 0.23 for the frontal cortex, indicating high specific tracer binding. Use of the arterial input function without metabolite correction resulted in a 10% underestimation in V_T, and was without important biasing effects on BP_{ND}.

☆ The asterisk applied in the receptor nomenclature notifies that the receptor complex may include additional subunits.

* Corresponding author at: Department of Nuclear Medicine, University of Leipzig, Liebigstraße 18, 04103 Leipzig, Germany.
E-mail address: Osama.Sabri@medizin.uni-leipzig.de (O. Sabri).

[1] Contributed equally.

http://dx.doi.org/10.1016/j.neuroimage.2015.05.065
1053-8119/

Altogether, kinetics and imaging properties of (−)-[^{18}F]Flubatine appear favorable and suggest that (−)-[^{18}F]Flubatine is a very suitable and clinically applicable PET tracer for in vivo imaging of α4β2* nAChRs in neuropsychiatric disorders.

Introduction

Neuronal nicotinic receptors (nAChRs) are ligand-gated ion channels that are physiologically activated by acetylcholine. Each receptor is composed of five cylindrical transmembrane subunits forming the central ion channel, and can be composed of α7 subunits or some stoichiometric combination of α and β subunits (α2–10, β2–4). The various forms are widely expressed throughout the brain. In the human brain, the most abundant form is the α4β2* subtype (Dani and Bertrand, 2007). The α4β2* nAChRs play an important role in normal brain function regulating a variety of brain processes such as mood, cognition and motor control (Changeux and Edelstein, 2005). Pathological alterations of the α4β2* nAChRs are thought to contribute to several psychiatric and neurological disorders (Dani and Bertrand, 2007; Mihailescu and Drucker-Colín, 2000; Perry et al., 1995; Rinne et al., 1991).

Noninvasive imaging using positron emission tomography (PET) or single-photon emission computer tomography (SPECT) has proved essential in the quantitative assessment of in vivo pathological changes of the α4β2* nAChR availability in neuropsychiatric disorders. High-affinity α4β2* nAChR specific radioligands, such as 5-[^{123}I]IA-85380 (5-IA) for SPECT and 6-[^{18}F]FA-85380 (6-FA) and 2-[^{18}F]FA-85380 (2-FA) for PET, have been developed and optimized for α4β2* nAChR imaging (Chefer et al., 1998; Ding et al., 2004; Doll et al., 1999; Horti et al., 1998; Kimes et al., 2003; Mamede et al., 2004; Scheffel et al., 2000; Schildan et al., 2007). Recently, through the use of 2-FA-PET and 5-IA-SPECT, cortical and subcortical abnormalities of the α4β2* nAChR binding have been reported in a variety of neuropsychiatric disorders such as Alzheimer's disease (AD) and mild cognitive impairment (MCI) (Kendziorra et al., 2011; O'Brien et al., 2007; Okada et al., 2013; Sabri et al., 2008), Parkinson's disease (PD) (Fujita et al., 2006; Kas et al., 2009; Meyer et al., 2009), epilepsy (Picard et al., 2006), nicotine dependence (Mukhin et al., 2008; Staley et al., 2006), major depressive disease (Saricicek et al., 2012), and schizophrenia (D'Souza et al., 2012; Brašić et al., 2012).

However, the slow kinetics of the PET radioligand 2-[^{18}F]FA-85380 and SPECT radioligand 5-[^{123}I]IA-85380 require lengthy acquisition times of up to 7 h to enable whole-brain nAChR analysis. Therefore, the use of 2-FA or 5-IA for large-scale clinical trials and routine clinical application may be limited (Horti and Villemagne, 2006; Horti et al., 2010; Sabri et al., 2008). A new generation α4β2* nAChR specific PET radioligands, such as (−)-[^{18}F]norchloro-fluoro-homoepibatidine ((−)-[^{18}F]NCFHEB), also known as (−)-[^{18}F]Flubatine, [^{18}F]AZAN and [^{18}F]nifene, demonstrating faster kinetic properties in both preclinical and in-man investigations have been developed (Brust et al., 2008; Hillmer et al., 2011; Hockley et al., 2013; Kuwabara et al., 2012; Sabri et al., 2008; Wong et al., 2013). We recently developed (−)-[^{18}F]Flubatine as a less toxic derivative of epibatidine (Bai et al., 1996; Brust et al., 2008; Deuther-Conrad et al., 2004, 2008; Fischer et al., 2013; Patt et al., 2003, 2013, 2014; Sabri et al., 2008; Smits et al., 2014). Preclinical studies demonstrated that (−)-[^{18}F]Flubatine has high selectivity and specificity for α4β2* nAChRs (Brust et al., 2008; Deuther-Conrad et al., 2004; Smits et al., 2014).

The objectives of the present study were to determine the safety and tolerability of (−)-[^{18}F]Flubatine, and to evaluate kinetic model-based approaches to quantify α4β2* nAChR binding parameters from dynamic PET and blood data in healthy volunteers.

Methods

Human subjects

Twelve healthy male volunteers (age: 71.0 ± 5.0 years, range: 63 to 76 years) took part in the study. All were non-smokers, drug free for any kind of centrally acting medication, and had no history of neurological or psychiatric illness. They were recruited by newspaper advertisement and from an existing database at the Max-Planck-Institute for Human Cognitive and Brain Sciences, Leipzig. All study subjects underwent a thorough clinical assessment, and were required to achieve results within one standard deviation of the mean in several psychometric tests. Other exclusion criteria were: hematological, biochemical or ECG parameters outside the normal range; a history of smoking, alcohol or drug abuse/addiction or major allergic reactions; any significant disease or unstable medical condition within the preceding twelve months; MRI contraindication; and clinically significant, abnormal physical examination or grossly pathological findings in the brain MRI. All subjects gave written informed consent. The clinical PET study was performed according to the 1964 Declaration of Helsinki and subsequent revisions and was approved by the local ethics committee as well as the national radiation protection and drug authorities. The trial is registered under EudraCT 2009-012408-26.

Radiochemistry

(−)-[^{18}F]Flubatine was prepared by aminopolyether-assisted nucleophilic substitution on a BOC-protected trimethylammonium precursor (Smits et al., 2014). The radiosynthesis was performed under GMP conditions using an automated synthesis module (Tracerlab FXFN, GE Medical Systems) within a synthesis time of 40 ± 2 min, with an average specific activity of 3×10^6 GBq/mmol (Patt et al., 2013).

PET and MR image acquisition and processing

Dynamic (−)-[^{18}F]Flubatine brain PET data were obtained in 3D scanning mode on an ECAT Exact HR+ scanner (CTI/Siemens, 63 slices, resolution 4.7 mm full width at half maximum [FWHM]) following the injection (90 s continuous short infusion [10 mL solution]) of 353.7 ± 9.4 MBq (−)-[^{18}F]Flubatine. Emission measurement consisted of one dynamic scan of 90 min and three subsequent static scans of 30 min each (resulting in a total scanning time of 270 min). PET data were corrected for scatter, attenuation (using a 10 min ^{68}Ge transmission scan acquired before the first emission scan), and radioactive decay, and reconstructed by ordered subset expectation maximization (OSEM) with 10 iterations and 16 subsets with a pixel size of 2.6 × 2.6 × 2.4 mm. In addition to the PET imaging, all subjects received a 3 T brain MRI (Magnetom Trio, Siemens Healthcare) for anatomical correlation and to exclude relevant pathologic findings. The MR imaging protocol included a T1-weighted magnetization prepared rapid gradient echo 3-dimensional sequence (MPRAGE; TR 2130 ms, TE 3,03 ms, TI 1200 ms, matrix 256 × 256 × 256, pixel bandwidth of 130 Hz) and a transverse T2-weighted turbo spin echo sequence. Image preprocessing before kinetic analysis was conducted using PMOD software (PMOD Technologies Ltd.; CH-8006 Zürich). The individual MRI data sets of the subjects were spatially reoriented onto a standard brain data set similar to the Talairach space. Volumes of interest (VOIs) within

29 brain regions were manually drawn in PMOD on three consecutive transversal slices (in rare cases two or four slices, if necessary) of the reoriented individual T1-weighted-MPRAGE data sets (Fig. 1). Outcome of PET data analysis was pooled for left and right hemispheres. In PET studies the corpus callosum is the region in the human brain with the lowest distribution volume, suggesting that there is only very low α4β2* nAChR density (Ding et al., 2004; Mukhin et al., 2008; Sabri et al., 2008; Wong et al., 2013). This is supported by a displacement PET study in tobacco smokers using the α4β2* nAChR specific radioligand 2-[^{18}F]F-A-85380. It was also revealed that 2-[^{18}F]F-A-85380 within the corpus callosum is almost non-displaceable by nicotine (Brody et al., 2006). For these reasons, we used the corpus callosum as the most suitable reference region to calculate the binding potential BP_{ND}. This region has been suggested for other α4β2* nAChR specific PET radioligands, such as 6-[^{18}F]F-A-85380 (Ding et al., 2004), 2-[^{18}F]F-A-85380 (Mukhin et al., 2008; Sabri et al., 2008), and [^{18}F]AZAN (Wong et al., 2013).

The dynamic PET data were corrected for motion artifacts using SPM2 software (SPM2-Software; Wellcome Trust Centre for Neuroimaging, University College London) and then co-registered with the individual MRI data (Hesse et al., 2012). Once registered, PMOD was used to produce the time–activity curves (TACs) necessary for kinetic analysis.

Blood sampling and plasma data analyses

For each subject 2 mL arterial blood samples were obtained. Ten to fifteen samples were acquired in the first 3 min following injection, with other samples taken at 3, 4, 5, 6, 8, 10, 12, 14, 16, 18, 20, 25, 30, 40, 50, 60, 70, 80, 90, 120, 150, 180, 210, 240, and 270 min post injection (p.i.). Additional samples of 5 mL for metabolite analysis were taken at 3, 10, 20, 30, 50, 70, 90, 120, 150, 210 and 270 min p.i. All samples were centrifuged to separate supernatant plasma from the remnants. The radioactivity in plasma aliquots was measured using a Cobra

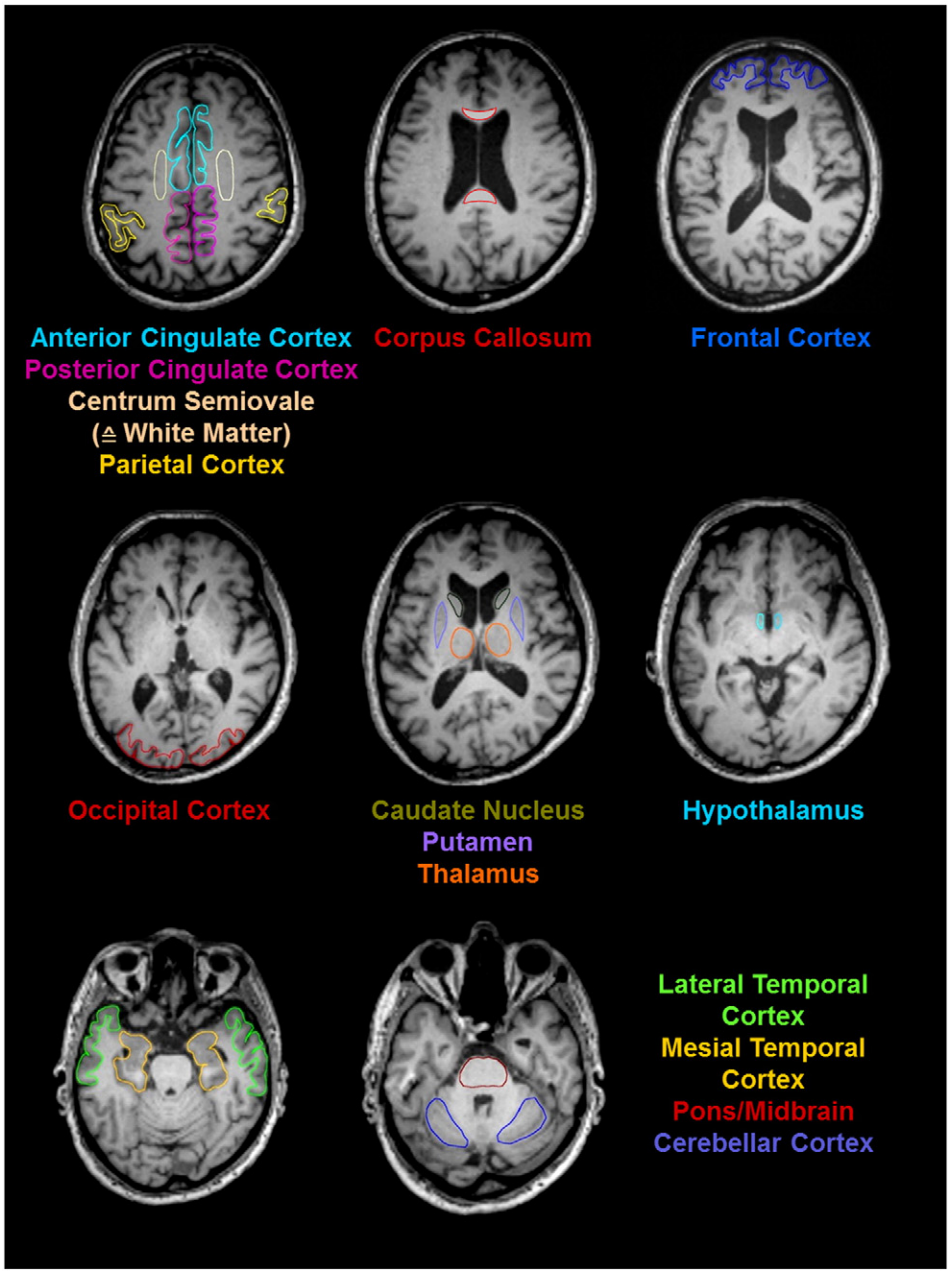

Fig. 1. Transaxial slices of MRI with all defined volumes of interest.

gamma counter (Packard Instrument Company, Meriden, CT, USA) and corrected for decay of ^{18}F.

Estimation of the non-metabolized parent fraction of the tracer was done as follows. The samples for metabolite analysis were deproteinized by precipitation with acetonitrile before being centrifuged. The resulting protein-free samples were then analyzed by radio high performance liquid chromatography (radio-HPLC). The fraction of non-metabolized (−)-[^{18}F]Flubatine was estimated by dividing the peak areas of (−)-[^{18}F]Flubatine in the radiochromatogram by the sum of all peaks. These ratios were fitted by a sum of 2 exponential functions and used to compute the metabolite-corrected arterial input function. Additionally, the free fraction of radiotracer in plasma (f_P) i.e., (−)-[^{18}F]Flubatine not bound to plasma proteins was determined for each subject by ultrafiltration as described previously (Sorger et al., 2006): In short, (−)-[^{18}F]Flubatine was added to samples of blood plasma at 37 °C and separated in plasma proteins and protein-free solution by ultrafiltration. Radioactivity was then estimated in both fractions with the gamma counter.

In addition we assessed the velocity of equilibration of (−)-[^{18}F]Flubatine between whole blood and plasma. To do this we added (−)-[^{18}F]Flubatine to whole blood samples of several volunteers, separated corpuscular blood components and plasma at different times by centrifugation and measured the amount of radioactivity in both fractions. The procedures and results of metabolite analysis, plasma protein binding and velocity of equilibration between whole blood and plasma were described in detail and published elsewhere (Patt et al., 2014). Metabolization of (−)-[^{18}F]Flubatine was very low, resulting in almost 90% unchanged parent compound at 90 min and 85% at 270 min p.i.

Kinetic data analysis and modeling

The generated VOI-based tissue time–activity curves (TACs) were used for kinetic analysis with 1- and 2-tissue compartment models (1TCM, 2TCM). To test the influence of the amount of metabolites in plasma on the kinetic modeling output parameters, two different arterial input functions were used: one with and one without individual metabolite correction. Results presented were computed with a metabolite-corrected input function, unless explicitly stated otherwise.

The 2TCM is described by the following differential equations:

$$\frac{dx_1(t)}{dt} = -(k_2 + k_3)x_1(t) + k_4 x_2(t) + K_1 c_a(t) \tag{1}$$

$$\frac{dx_2(t)}{dt} = k_3 x_1(t) - k_4 x_2(t) \tag{2}$$

where $x_1(t)$ is the time-dependent concentration of free and nonspecifically bound tracer, $x_2(t)$ the concentration of specifically receptor bound tracer and $c_a(t)$ the arterial input function. K_1 (mL cm^{-3} min^{-1}) describes the transport from blood plasma to the first tissue compartment, k_2 (min^{-1}) vice versa; k_3 (min^{-1}) and k_4 (min^{-1}) describes the association and dissociation at resp. from the receptor. The unit of tissue tracer concentrations is (kBq cm^{-3}). The total distribution volume V_T (mL cm^{-3}) is given by

$$\frac{K_1}{k_2}\left(1 + \frac{k_3}{k_4}\right) = \frac{K_1}{k_2}\left(1 + \frac{f_{ND} B_{avail}}{K_D}\right) \tag{3}$$

and the binding potential BP_{ND} can be computed using a receptor-free reference region according to

$$BP_{ND} = V_T / V_{reference} - 1 = f_{ND} B_{avail} / K_D. \tag{4}$$

Here B_{avail} (nM) is the concentration of nAChRs available for the tracer and f_{ND} the free fraction of tracer in the first (nondisplaceable) tissue compartment. K_D (nM) is the equilibrium dissociation constant of the radioligand/receptor system (Innis et al., 2007).

The differential equation for the 1TCM is given by

$$\frac{dx_1(t)}{dt} = K_1 c_a(t) - k_2' x_1 \tag{5}$$

and solved by the convolution integral

$$x_1(t) = K_1 e^{-k_2' t} \otimes c_a(t) = K_1 \int_0^t e^{-k_2'(t-\tau)} c_a(\tau) d\tau, \ (\otimes \text{ for convolution}). \tag{6}$$

The total distribution volume V_T of the 1TCM is computed according to

$$V_T = K_1 / k_2'. \tag{7}$$

Rate constants of the 1TCM, 2TCM as well as the fractional blood volume V_b were estimated by minimizing a nonlinear least-squares cost function of the sum of squared differences between measured PET tracer concentrations and model predictions (Bertoldo and Cobelli, 2014). Standard errors of the parameters and coefficients of variation (COV) were computed from the covariance matrix of the cost function.

In addition, parametric images of the regional (−)-[^{18}F]Flubatine distribution volume were calculated using the Logan plot (11 points between 13 to 90 min p.i.) with the arterial input function (Logan et al., 1990). The starting point of 13 min in the Logan plot analysis was used since linearity in the Logan plot was reached after approximately 10 min in the thalamus as the region with the highest α4β2* nAChR density.

Statistical analyses

Kinetic modeling parameters are expressed as mean value ± standard deviation (SD). For model selection between the 1- and 2-tissue compartment models we used the Akaike's information criterion (AICc) with correction for small sample size (Burnham and Anderson, 2002; Turkheimer et al., 2003). In case of nonlinear residual sum of squares (RSS) minimization, the AICc is given by

$$\text{AICc} = n \log\left(\frac{\text{RSS}}{n}\right) + 2k + \frac{2k(k+1)}{n-k-1} \tag{8}$$

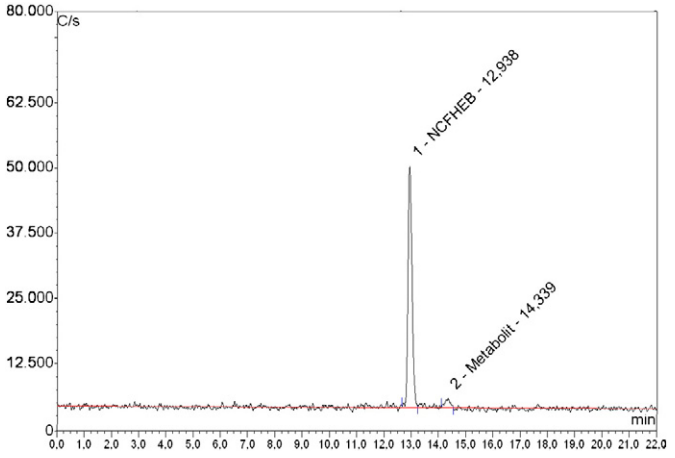

Fig. 2. Approximately 95% of injected (−)-[^{18}F]Flubatine stayed intact as shown by chromatographic analysis 20 min p.i.. Degradation of the tracer was very low; resulting in almost 90% unchanged parent compound at 90 min and 85% at 270 min p.i. The retention time (min) of a peak is given adjacent to the peak identification.

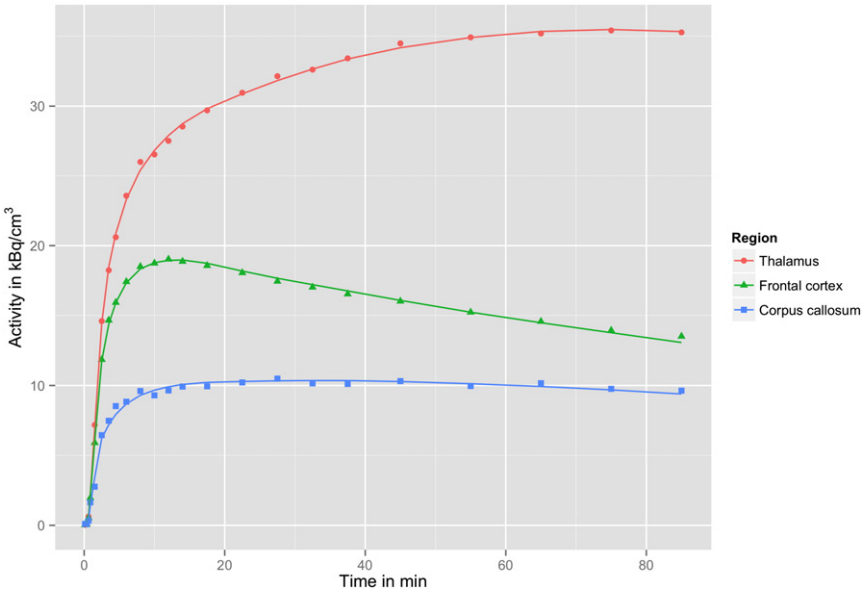

Fig. 3. 1-tissue compartment model fits of 90 min measured time–activity curves in thalamus, frontal cortex and corpus callosum of one healthy subject.

where n is the sample size (number of frames, n = 23), k the number of estimated model parameters + 1 ($k = 4, 6$) and log the natural logarithm. Statistical analyses were performed with MATLAB (version 7.3 (R2006b), the MathWorks, Natick, MA, USA) and IBM SPSS statistic software, version 20.

Results

Blood plasma and kinetic analyses

In blood plasma, almost 90% of unchanged (−)-[^{18}F]Flubatine as measured by radio-HPLC was found at 90 min and 85% at 270 min p.i. (Patt et al., 2014). This demonstrates that (−)-[^{18}F]Flubatine is very stable (Fig. 2). Notably, in an animal study (juvenile female pigs) we measured about 60% metabolites in plasma at 90 min after injection of (−)-[^{18}F]Flubatine (Brust et al., 2008). Please note that in this reference the older name (−)-[^{18}F]NCFHEB is used. Plasma protein binding was 15.2 ± 1.0%. Equilibration of (−)-[^{18}F]Flubatine between whole blood and blood plasma was virtually instantaneous and did not change significantly over time, i.e., a time dependence of the concentration of the parent compound due to slow transport into erythrocytes did not have to be considered. The respective value was approximately 73% (plasma/whole blood). In the brain, the tracer showed fast kinetics; pseudo equilibrium was reached within 90 min p.i. in the thalamus (maximum of the TAC). Estimation of kinetic parameters for all brain regions with 1TCM was possible within this time frame (30 min p.i. for all cortical regions; Figs. 3 and 4). In cortical regions, pseudo equilibrium was reached within 15 min p.i. (Fig. 3).

(−)-[^{18}F]Flubatine plasma time–activity curves showed an early initial peak and a very slow decrease until 270 min (Patt et al., 2014). A

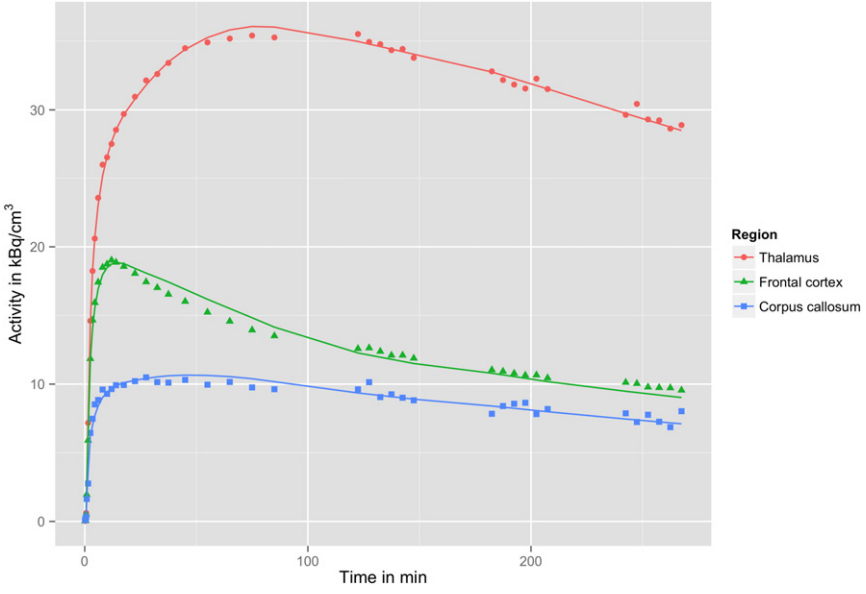

Fig. 4. 1-tissue compartment model fits of 270 min measured time–activity curves in thalamus, frontal cortex and corpus callosum of one healthy subject.

similar behavior was observed in brain tissue; where after reaching the tracer activity peak, a slow decrease of tracer concentration was detected (time range 0–90 min [Fig. 3] or 0–270 min [Fig. 4]).

Model selection

Using an input function without metabolite correction the Akaike's information criterion AICc favored the 1TCM in the thalamus in 6 volunteers, in the frontal cortex in 3 volunteers and in the corpus callosum again in 6 of the 12 subjects, i.e., the AICc computed with the 1TCM had lower values. The mean AICc of the 12 subjects of both models was similar in thalamus (1TCM: −34.2 ± 12.9; 2TCM: −37.0 ± 12.5) and corpus callosum (1TCM: −44.2 ± 10.3; 2TCM: −46.3 ± 8.5) but lower for the 2TCM in the frontal cortex (1TCM: −62.3 ± 20.2; 2TCM: −77.3 ± 10.95).

Employing the metabolite-corrected input function led to similar results in model selection for the thalamus and corpus callosum. The AICc favored the 1TCM in the thalamus in 5 volunteers and in the corpus callosum in 4 of the 12 subjects. The mean AICc of the 2TCM was only slightly lower in thalamus (1TCM: −34.1 ± 11.4; 2TCM: −36.9 ± 12.4) and corpus callosum (1TCM: −43.1 ± 9.7; 2TCM: −46.3 ± 8.6). For the frontal cortex, however, AIC always chose the 2TCM and the mean AICc of the 2TCM was 23.7 lower (1TCM: −53.9 ± 15.9; 2TCM: −77.6 ± 10.96). Use of the AICc to compare the 1TCM with and without metabolite-corrected input function in the frontal cortex favored the non metabolite-corrected input function approach in 10 of the 12 subjects investigated in this study.

Quantitative (−)-[^{18}F]Flubatine PET imaging data

V_T obtained by the 1TCM was similar for the 0–90 min period and the 0–270 min time range (Table 2). The variation between the corresponding fit data is probably mainly due to subject head repositioning (Figs. 3 and 4) and errors in the measurements of metabolites at late time points.

V_T values were highest in the thalamus regions (27.44 ± 3.77), intermediate in regions like midbrain, striatum and cerebellum (e.g., putamen: 12.70 ± 0.87), slightly lower in cortical regions (e.g., frontal cortex: 10.02 ± 0.83), and lowest in the corpus callosum (6.31 ± 0.80) — as expected from known receptor densities (Brody et al., 2006; Paterson and Nordberg, 2000) and indicated in Table 1. In vitro measurements of regional nAChR densities in postmortem human brain tissue using (±)-[^{3}H]epibatidine (Marutle et al., 1998) and V_T of (−)-[^{18}F]Flubatine as obtained in this present study (Table 1) were highly correlated (Fig. 5, $r = 0.98$, $p < 0.001$) despite differences in nAChR subtype specificity of both tracers (Deuther-Conrad et al., 2004).

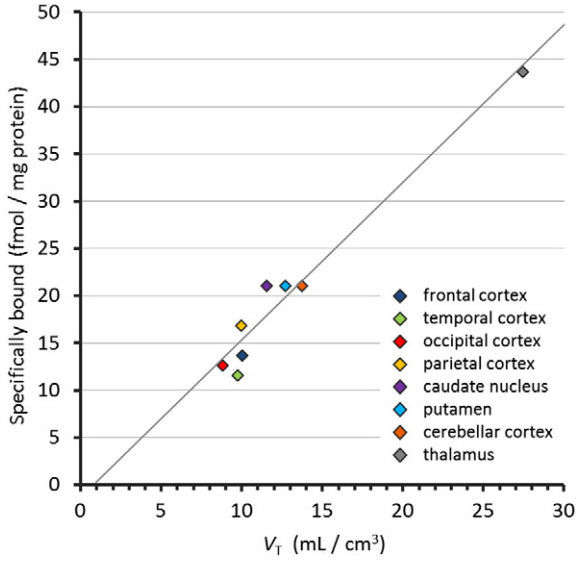

Fig. 5. Linear regression analysis of specific (±)-[^{3}H]epibatidine binding as reported by Marutle et al. (1998) vs. V_T of (−)-[^{18}F]Flubatine in 8 human brain regions (thalamus, caudate nucleus, putamen, cerebellar cortex, parietal, frontal, occipital and temporal cortices) ($r = 0.98$, $p < 0.001$, specifically_bound = 1.66·V_T–1.38).

Coefficients of variation of V_T were <5% in thalamus and cortical regions, demonstrating robust parameter estimation (thalamus: 2.3% ± 0.6%; frontal cortex: 1.5 ± 0.6%). The BP_{ND}, calculated with the corpus callosum as reference region, was 3.41 ± 0.79 for the thalamus, 1.04 ± 0.25 for the putamen, and 0.61 ± 0.23 for the frontal cortex.

V_T was reliably estimated from 60 min and even from 30 min dynamic PET data (Table 2). Mean regional V_T values calculated from 90 min fit data were only slightly higher (between 5–10%) than those calculated from 30 min fit data.

Furthermore, V_T as computed by the 2TCM was in good agreement with the 1TCM values (Table 1). However, the relative standard deviation of V_T using a 2TCM was much larger.

Results without metabolite correction

Use of an uncorrected input function yielded slightly (about 10%) lower distribution volumes for all regions, due to the fact that the

Table 1
Quantitative (−)-[^{18}F]Flubatine PET parameters in selected brain regions.

Brain region	K_1	k_2'	V_T	BP_{ND}	V_T (2TCM)
Frontal cortex	0.37 ± 0.04	0.037 ± 0.003	10.02 ± 0.83	0.61 ± 0.23	10.43 ± 1.29
Lateral temporal cortex	0.33 ± 0.03	0.034 ± 0.003	9.74 ± 0.68	0.56 ± 0.20	9.98 ± 1.02
Mesial temporal cortex	0.30 ± 0.03	0.030 ± 0.003	10.11 ± 0.93	0.62 ± 0.23	10.48 ± 1.27
Parietal cortex	0.37 ± 0.04	0.037 ± 0.004	9.96 ± 0.93	0.60 ± 0.22	10.29 ± 1.31
Occipital cortex	0.37 ± 0.04	0.042 ± 0.004	8.81 ± 0.50	0.42 ± 0.18	9.09 ± 0.79
Anterior cingulate cortex	0.33 ± 0.05	0.034 ± 0.003	9.81 ± 0.93	0.57 ± 0.19	10.10 ± 1.14
Posterior cingulate cortex	0.39 ± 0.06	0.038 ± 0.004	10.25 ± 0.80	0.64 ± 0.16	10.55 ± 0.92
Caudate nucleus	0.42 ± 0.04	0.036 ± 0.004	11.54 ± 0.98	0.85 ± 0.26	11.83 ± 1.16
Putamen	0.45 ± 0.05	0.036 ± 0.005	12.70 ± 0.87	1.04 ± 0.25	12.86 ± 1.33
Thalamus	0.50 ± 0.07	0.018 ± 0.003	27.44 ± 3.77	3.41 ± 0.79	27.59 ± 4.19
White matter	0.16 ± 0.01	0.016 ± 0.002	10.74 ± 1.40	0.73 ± 0.31	11.96 ± 2.39
Pons/midbrain	0.32 ± 0.04	0.027 ± 0.004	12.18 ± 1.20	0.96 ± 0.33	12.43 ± 1.93
Cerebellar cortex	0.43 ± 0.06	0.032 ± 0.004	13.73 ± 1.66	1.20 ± 0.37	13.86 ± 1.96
Corpus callosum	0.15 ± 0.02	0.025 ± 0.002	6.31 ± 0.80	n.a.	6.78 ± 0.93
Hypothalamus	0.31 ± 0.04	0.023 ± 0.003	13.59 ± 2.43	1.18 ± 0.45	13.82 ± 2.46

All parameters were estimated from 90 min PET data. Parameters of the 1-tissue compartmental modeling: K_1: influx constant, k_2': washout constant, V_T: distribution volume, BP_{ND}: binding potential. V_T was additionally computed by 2-tissue compartmental modeling. In both cases, metabolite-corrected arterial input functions were used. Values are given as mean value ± standard deviation.

Table 2
Influence of dynamic PET scan duration on regional (−)-[^{18}F]Flubatine distribution volumes.

Brain region	V_T (30 min)	V_T (60 min)	V_T (90 min)	V_T (270 min)
Frontal cortex	9.32 ± 0.70	9.76 ± 0.74	10.02 ± 0.83	10.61 ± 0.98
Lateral temporal cortex	9.26 ± 0.69	9.59 ± 0.65	9.74 ± 0.68	10.02 ± 0.73
Mesial temporal cortex	9.48 ± 0.90	9.91 ± 0.85	10.11 ± 0.93	10.52 ± 0.93
Parietal cortex	9.38 ± 0.89	9.74 ± 0.86	9.98 ± 0.93	10.55 ± 1.08
Occipital cortex	8.16 ± 0.42	8.58 ± 0.45	8.81 ± 0.50	9.31 ± 0.63
Anterior cingulate cortex	9.06 ± 0.94	9.53 ± 0.93	9.81 ± 0.93	10.61 ± 0.78
Posterior cingulate cortex	9.53 ± 0.86	9.98 ± 0.80	10.25 ± 0.79	10.98 ± 0.72
Caudate nucleus	10.93 ± 1.06	11.26 ± 0.96	11.54 ± 0.98	12.39 ± 1.08
Putamen	11.94 ± 0.80	12.36 ± 0.72	12.70 ± 0.87	14.12 ± 1.52
Thalamus	25.53 ± 3.63	26.84 ± 3.55	27.44 ± 3.77	29.36 ± 3.97
White matter	8.94 ± 1.21	10.03 ± 1.24	10.74 ± 1.40	12.63 ± 1.56
Pons/midbrain	11.54 ± 1.25	11.97 ± 1.02	12.18 ± 1.20	12.43 ± 1.26
Cerebellar cortex	13.16 ± 1.61	13.56 ± 1.60	13.73 ± 1.66	13.85 ± 1.84
Corpus callosum	5.56 ± 0.90	6.03 ± 0.84	6.31 ± 0.80	6.86 ± 0.75
Hypothalamus	12.11 ± 2.38	13.05 ± 2.27	13.59 ± 2.43	14.52 ± 2.97

Distribution volumes V_T were obtained by 1-tissue compartmental modeling using metabolite-corrected arterial input functions. Values are given as mean value ± standard deviation.

uncorrected input function at 90 min is about 10% higher (Table 3). The relative standard deviation of V_T was lower with input functions without metabolite correction (frontal cortex: 21%, thalamus: 12%). BP_{ND} values computed with and without metabolite correction were in excellent agreement (Tables 1 and 3). V_T values computed by Logan plots (Table 3) were lower than those obtained by 1TCM (frontal cortex: 7%, thalamus: 11%).

Parametric images of V_T (obtained by Logan graphical analysis) demonstrate high image quality in one healthy subject with abundant α4β2* nAChR binding throughout the cortex and subcortical structures (Fig. 6).

Safety evaluation

There were no adverse effects from the tracer. At the time of injection, the administered amount of the radioligand was equivalent to a mass dose of 0.074 ± 0.077 μg. The "No Observed Adverse Effect Level (NOEL)" of (−)-[^{18}F]Flubatine was estimated to 6.2 μg/kg (body weight) in animal experiments (Wistar rats; Harlan Laboratories, Itingen, Switzerland); therefore the injected dose was approximately 5000 times lower than the NOEL.

Discussion

This study describes the first-in-human application of a new PET tracer (−)-[^{18}F]Flubatine, developed as a viable alternative to the slow tracer kinetic PET and SPECT radioligands 2-[^{18}F]FA-85380 and 5-[^{123}I]IA-85380. (−)-[^{18}F]Flubatine is a less toxic derivative of epibatidine with favorable preclinical results in terms of α4β2* nAChR specificity and selectivity (Brust et al., 2008; Deuther-Conrad et al., 2004, 2008; Gallezot et al., 2014; Hockley et al., 2013).

Several other PET tracers for α4β2* nAChR have recently been developed aiming for shorter acquisition times (for review see for example Horti et al., 2013; Mo et al., 2014). However, only [^{18}F]AZAN has been successfully applied for the measurement of α4β2* nAChRs in the human brain. These measurements indicate that 90 min PET scans are sufficient to estimate BP_{ND} in receptor-rich brain regions (Wong et al., 2013).

This first clinical (−)-[^{18}F]Flubatine trial demonstrates that the favorable preclinical characteristics of the tracer translates to humans. That is: (1) high cortical brain uptake as shown by high cortical tracer delivery rate constants K_1 (>0.3 mL cm^{-3} min^{-1}), (2) fast kinetics, and (3) the possibility to estimate V_T by a simple 1TCM within 90 min for all regions of interest used here, or even within 30 min for all cortical regions (Becker et al., 2012; Sabri et al., 2012). When applying a 2TCM instead, two more rate constants k_3, k_4 need to be estimated from the data. However, if the 1TCM already allows for a good description of the data then not all 4 rate constants K_1, …, k_4 are a posteriori identifiable (i.e., estimable with sufficient precision). As a consequence, attempts to estimate all rate constants in this situation result in large coefficients of variation for k_2, k_3, and k_4. This reflects the fact that these 3 parameters are not independent of each other, but related by $k_2' = k_2/(1 + k_3/k_4)$ (Eqs. (3) and (7)). Only K_1 and V_T are a posteriori identifiable from the data. It should be added here that Akaike's information criterion does not distinctly favor the 1TCM or 2TCM for kinetic analysis. However, the total distribution volume V_T, which we computed with the 2TCM, was also estimated with lower precision. V_T is the crucial parameter here since it is a linear function of the receptor density. There is a substantial increase in the standard deviation of V_T in cortical regions (frontal cortex: 56%) and also to a lesser degree in the thalamus (10%) and the corpus callosum (16%) when using the 2TCM. Therefore, if V_T is to be the primary outcome measure of future trials, i.e., for employing (−)-[^{18}F]Flubatine to detect potential reductions of α4β2* nAChR densities in Alzheimer's or Parkinson's disease, then 1TCM is preferred over the 2TCM.

In the thalamus a 1TCM is especially appropriate. We assume that a fast equilibration of free and receptor-bound tracer in tissue occurs at a rate beyond the temporal resolution afforded by PET. The two parameters K_1 and k_2' of a one-compartment system can be reliably estimated

Table 3
Comparison of (−)-[^{18}F]Flubatine kinetic parameters as computed by 1-tissue compartmental modeling and the Logan plot.

Brain region	K_1	k_2'	V_T	BP_{ND}	V_T (Logan)
Frontal cortex	0.36 ± 0.03	0.040 ± 0.003	9.04 ± 0.59	0.63 ± 0.23	8.43 ± 0.50
Lateral temporal cortex	0.33 ± 0.03	0.038 ± 0.003	8.79 ± 0.52	0.58 ± 0.20	8.21 ± 0.41
Mesial temporal cortex	0.30 ± 0.03	0.033 ± 0.003	9.08 ± 0.68	0.64 ± 0.24	8.35 ± 0.55
Parietal cortex	0.37 ± 0.04	0.041 ± 0.004	8.99 ± 0.70	0.62 ± 0.22	8.32 ± 0.58
Occipital cortex	0.37 ± 0.04	0.046 ± 0.004	7.98 ± 0.39	0.44 ± 0.19	7.49 ± 0.32
Anterior cingulate cortex	0.33 ± 0.05	0.037 ± 0.004	8.83 ± 0.70	0.59 ± 0.20	8.15 ± 0.58
Posterior cingulate cortex	0.39 ± 0.06	0.041 ± 0.004	9.26 ± 0.63	0.66 ± 0.16	8.54 ± 0.51
Caudate nucleus	0.41 ± 0.04	0.039 ± 0.004	10.41 ± 0.76	0.88 ± 0.27	9.74 ± 0.80
Putamen	0.44 ± 0.05	0.039 ± 0.005	11.45 ± 0.68	1.06 ± 0.25	10.51 ± 0.55
Thalamus	0.49 ± 0.06	0.020 ± 0.003	24.16 ± 2.91	3.36 ± 0.79	21.58 ± 2.53
White matter	0.16 ± 0.01	0.017 ± 0.002	9.34 ± 0.99	0.69 ± 0.30	8.35 ± 1.07
Pons/midbrain	0.32 ± 0.04	0.029 ± 0.004	10.90 ± 0.94	0.97 ± 0.33	10.07 ± 0.79
Cerebellar cortex	0.43 ± 0.05	0.035 ± 0.004	12.34 ± 1.32	1.22 ± 0.38	11.25 ± 1.12
Corpus callosum	0.15 ± 0.02	0.027 ± 0.003	5.63 ± 0.74	n.a.	5.26 ± 0.76
Hypothalamus	0.30 ± 0.04	0.025 ± 0.003	12.07 ± 2.03	1.17 ± 0.45	11.26 ± 1.84

All data were obtained from 90 min PET scans. No metabolite corrections of the arterial input functions were applied. Values are given as mean ± standard deviation.

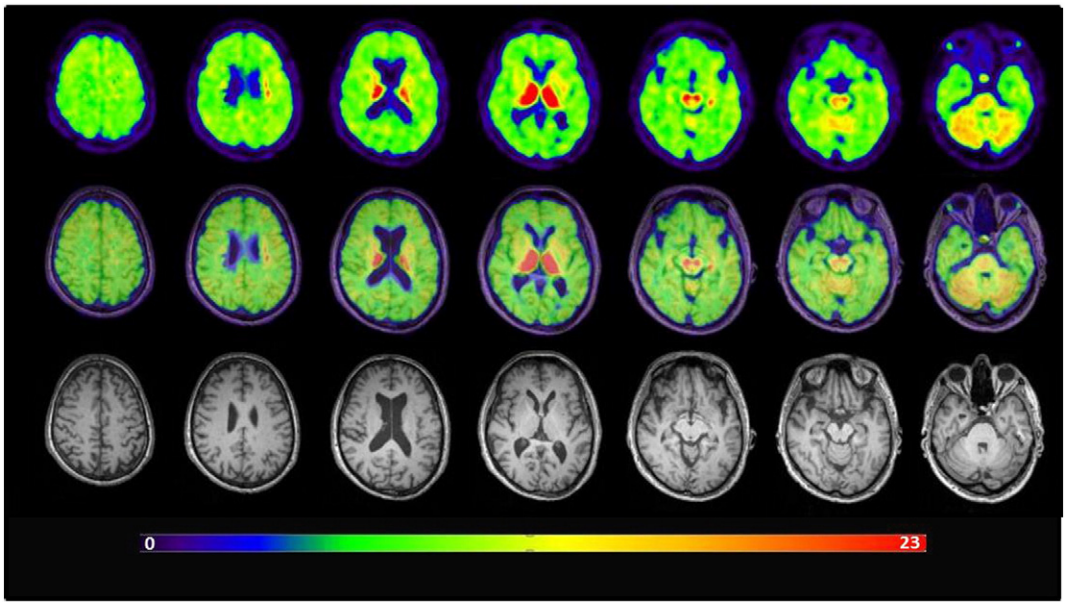

Fig. 6. Parametric images of the distribution volume V_T (obtained by Logan graphical analysis) of (−)-[^{18}F]Flubatine PET in one healthy subject show high image quality and reflect the known distribution of α4β2* nicotinic acetylcholine receptors (α4β2* nAChRs) in the brain. Transaxial PET images of V_T (upper row), PET/MRI (image fusion; middle row) and T1-MRI data (lower row) are shown. Following the normal distribution of α4β2* nAChR availability, the values of V_T are high within the thalamus, moderate within the striatum, midbrain and cerebellum, relatively low within the cortex and extra-callosal white matter, and very low within the corpus callosum.

and the measuring time can thus be reduced to 90 min or even less depending on V_T (i.e., depending on the receptor concentration in a brain region).

In addition, due to the low level of metabolites formed (Patt et al., 2014), the use of an arterial input function that is not corrected for metabolites seems to be an attractive and simpler approach that does not reduce the sensitivity in a group comparison. Estimation of metabolites is error-prone and is an unreliable factor when calculating the arterial input function. Using an input function without metabolite correction only reduced V_T by approximately 10%, although further studies comparing this feature between diseased and healthy subjects are still required. The same holds for correction of the free fraction in plasma f_P. In a previous study, the values of f_P did not differ between patients with Alzheimer's disease and healthy controls (Patt et al., 2014).

These issues notwithstanding, the tracer showed a fast velocity of equilibration between plasma and whole blood as well as moderate plasma protein binding which also facilitates kinetic analysis.

In summary, (−)-[^{18}F]Flubatine can be described with a 1TCM, shows low metabolite formation, and V_T can be estimated in cortical regions from PET recordings of only 30 min duration and in all other regions from PET recordings of 90 min. In cortical regions, pseudo-equilibrium of the tracer between brain tissue and plasma is reached at about 20 min p.i. and at subsequent times the tracer concentrations in tissue and plasma decrease in parallel very slowly. Therefore sufficient information to estimate K_1, k_2' with the 1TCM is present in this very short time frame for the case of cortex, whereas later PET frames depict repeated measurements of the tissue to plasma ratio at steady state. This explains the surprisingly short time needed to compute V_T. Repeated measurements at steady-state conditions reduce the standard error of V_T. But this can be counterbalanced with an increase of measurement errors due to e.g., an increase of head movements at longer PET scans. Group standard deviations of V_T are very similar for PET recordings between 30 and 90 min (Table 1) so that optimal scan duration can be expected in this time range. This optimal short time interval also depends on the receptor density of a brain region and should be finally determined from the comparison of two groups of subjects with a known difference in nAChR density. Furthermore, the safety profile, together with recently published favorable dosimetry data (Sattler et al., 2014) indicate that (−)-[^{18}F]Flubatine is a safe and well tolerated radiopharmaceutical. We believe therefore that (−)-[^{18}F]Flubatine is a very capable tracer for α4β2* nAChR PET imaging, which is well suited for future clinical studies of normal human brain function and neuropsychiatric diseases.

Conclusion

In this study we have shown that (−)-[^{18}F]Flubatine can produce quantitative PET measurements of α4β2* nAChR availability in the human brain. It offers several advantages. Because metabolization of the tracer is small, it is not necessary to correct the arterial input function for metabolites. Binding to plasma proteins is also of minor importance, and because the free fraction of (−)-[^{18}F]Flubatine in plasma is uniformly high, a correction of V_T for f_P can also be omitted. The kinetics of (−)-[^{18}F]Flubatine are well described by a simple 1TCM. Indeed, given the lower precision of V_T when estimated using the 2TCM, the 1TCM is preferred for kinetic analysis. Finally, V_T computed from regional TACs can be robustly estimated in all cortical regions within a scan length of only 30 min, although we recommend 90 min of PET imaging until such time that more data become available. The option of shorter acquisition times compared to other α4β2* nAChR radiotracers is very important for clinical trials on challenging patients such as those with Alzheimer's disease.

Acknowledgments

The study was supported by a BMBF grant (German Federal Ministry of Education and Research; 01EZ0820, 01EZ0821, 01EZ0822 and 01EZ0823). S.G. received funding from the International Max Planck Research School on Neuroscience of Communication (IMPRS NeuroCom). We wish to thank all volunteers who participated in this trial. We are also grateful to the cyclotron, PET radiochemistry, and PET scanner crews of the Leipzig University Department of Nuclear Medicine for their skillful support. We are especially thankful to John Dickson (University College London Hospital, London, UK) and Mohammed Hankir (University of Leipzig, Leipzig, Germany) for careful line editing and English proofreading of the manuscript.

Conflict of interest

Swen Hesse is supported by the German Ministry of Education and Research (BMBF, Grant Number 01EO1001). Dr. Hoepping and Dr. Smits are employees of ABX advanced biochemical compounds. The other authors have no disclosures related to the study.

References

Bai, D., Xu, R., Chu, G., Zhu, X., 1996. Synthesis of (+/−)-epibatidine and its analogues. J. Org. Chem. 61, 4600–4606.

Becker, G., Wilke, S., Schoenknecht, P., Patt, M., Luthardt, J., Hesse, S., Wagenknecht, G., Hoepping, A., Brust, P., Sabri, O., 2012. PET quantification of (−)-[F-18]-flubatine binding to nicotinic alpha4beta2 acetylcholine receptors in human brains. J. Cereb. Blood Flow Metab. 32, S172–S173.

Bertoldo, A., Cobelli, C., 2014. Physiological modelling of positron emission tomography images. In: Carson, E., Cobelli, C. (Eds.), Modelling Methodology for Physiology and Medicine, 2nd ed. Elsevier, London, pp. 417–448.

Brašić, J.R., Cascella, N., Kumar, A., Zhou, Y., Hilton, J., Raymont, V., Crabb, A., Guevara, M.R., Horti, A.G., Wong, D.F., 2012. Positron emission tomography experience with 2-[^{18}F]fluoro-3-(2(S)-azetidinylmethoxy)pyridine (2-[^{18}F]FA) in the living human brain of smokers with paranoid schizophrenia. Synapse 66, 352–368.

Brody, A.L., Mandelkern, M.A., London, E.D., Olmstead, R.E., Farahi, J., Scheibal, D., Jou, J., Allen, V., Tiongson, E., Chefer, S.I., Koren, A.O., Mukhin, A.G., 2006. Cigarette smoking saturates brain α4β2 nicotinic acetylcholine receptors. Arch. Gen. Psychiatry 63, 907–915.

Brust, P., Patt, J.T., Deuther-Conrad, W., Becker, G., Patt, M., Schildan, A., Sorger, D., Kendziorra, K., Meyer, P., Steinbach, J., Sabri, O., 2008. In vivo measurement of nicotinic acetylcholine receptors with [^{18}F]norchloro-fluoro-homoepibatidine. Synapse 62, 205–218.

Burnham, K.P., Anderson, D.R., 2002. Model Selection and Multimodel Inference: A Practical Information Theoretic Approach. 2nd ed. Springer, New York, NY, pp. 70–75.

Changeux, J.-P., Edelstein, S.J., 2005. Nicotinic Acetylcholine Receptors. Odile Jacob Publishing Corporation, New York, NY, pp. 192–211.

Chefer, S.I., Horti, A.G., Lee, K.S., Koren, A.O., Jones, D.W., Gorey, J.G., Links, J.M., Mukhin, A.G., Weinberger, D.R., London, E.D., 1998. In vivo imaging of brain nicotinic acetylcholine receptors with 5-[^{123}I]iodo-A-85380 using single photon emission computed tomography. Life Sci. 63, L355–L360.

Dani, J.A., Bertrand, D., 2007. Nicotinic acetylcholine receptors and nicotinic cholinergic mechanisms of the central nervous system. Annu. Rev. Pharmacol. Toxicol. 47, 699–729.

Deuther-Conrad, W., Patt, J.T., Feuerbach, D., Wegner, F., Brust, P., Steinbach, J., 2004. Norchloro-fluoro-homoepibatidine: specificity to neuronal nicotinic acetylcholine receptor subtypes in vitro. Farmaco 59, 785–792.

Deuther-Conrad, W., Patt, J.T., Lockman, P.R., Allen, D.D., Patt, M., Schildan, A., Ganapathy, V., Steinbach, J., Sabri, O., Brust, P., 2008. Norchloro-fluoro-homoepibatidine (NCFHEB) — a promising radioligand for neuroimaging nicotinic acetylcholine receptors with PET. Eur. Neuropsychopharmacol. 18, 222–229.

Ding, Y.S., Fowler, J.S., Logan, J., Wang, G.J., Telang, F., Garza, V., Biegon, A., Pareto, D., Rooney, W., Shea, C., Alexoff, D., Volkow, N.D., Vocci, F., 2004. 6-[^{18}F]Fluoro-A-85380, a new PET tracer for the nicotinic acetylcholine receptor: studies in the human brain and in vivo demonstration of specific binding in white matter. Synapse 53, 184–189.

Doll, F., Dolci, L., Valette, H., Hinnen, F., Vaufrey, F., Guenther, I., Fuseau, C., Coulon, C., Bottlaender, M., Crouzel, C., 1999. Synthesis and nicotinic acetylcholine receptor in vivo binding properties of 2-fluoro-3-[2(S)-2-azetidinylmethoxy]pyridine: a new positron emission tomography ligand for nicotinic receptors. J. Med. Chem. 42, 2251–2259.

D'Souza, D.C., Esterlis, I., Carbuto, M., Krasenics, M., Seibyl, J., Bois, F., Pittman, B., Ranganathan, M., Cosgrove, K., Staley, J., 2012. Lower ß2*-nicotinic acetylcholine receptor availability in smokers with schizophrenia. Am. J. Psychiatry 169, 326–334.

Fischer, S., Hiller, A., Smits, R., Hoepping, A., Funke, U., Wenzel, B., Cumming, P., Sabri, O., Steinbach, J., Brust, P., 2013. Radiosynthesis of racemic and enantiomerically pure (−)-[18F]flubatine—a promising PET radiotracer for neuroimaging of α4β2 nicotinic acetylcholine receptors. Appl. Radiat. Isot. 74, 128–136.

Fujita, M., Ichise, M., Zoghbi, S.S., Liow, J.S., Ghose, S., Vines, D.C., Sangare, J., Lu, J.Q., Cropley, V.L., Iida, H., Kim, K.M., Cohen, R.M., Bara-Jimenez, W., Ravina, B., Innis, R.B., 2006. Widespread decrease of nicotinic acetylcholine receptors in Parkinson's disease. Ann. Neurol. 59, 174–177.

Gallezot, J.D., Esterlis, I., Bois, F., Zheng, M.Q., Lin, S.F., Kloczynski, T., Krystal, J.H., Huang, Y., Sabri, O., Carson, R.E., Cosgrove, K.P., 2014. Evaluation of the sensitivity of the novel α4β2* nicotinic acetylcholine receptor PET radioligand (18) F-(−)-NCFHEB to increases in synaptic acetylcholine levels in rhesus monkeys. Synapse 68, 556–564.

Hesse, S., Brust, P., Mäding, P., Becker, G.A., Patt, M., Seese, A., Sorger, D., Zessin, J., Meyer, P.M., Lobsien, D., Laudi, S., Habermann, B., Füchtner, F., Luthardt, J., Bresch, A., Steinbach, J., Sabri, O., 2012. Imaging of the brain serotonin transporters (SERT) with ^{18}F-labelled fluoromethyl-McN5652 and PET in humans. Eur. J. Nucl. Med. Mol. Imaging 39, 1001–1011.

Hillmer, A.T., Wooten, D.W., Moirano, J.M., Slesarev, M., Barnhart, T.E., Engle, J.W., Nickles, R.J., Murali, D., Schneider, M.L., Mukherjee, J., Christian, B.T., 2011. Specific α4β2 nicotinic acetylcholine receptor binding of [F-18]nifene in the rhesus monkey. Synapse 65, 1309–1318.

Hockley, B.G., Stewart, M.N., Sherman, P., Quesada, C., Kilbourn, M.R., Albin, R.L., Scott, P.J., 2013. (−)-[^{18}F]Flubatine: evaluation in rhesus monkeys and a report of the first fully automated radiosynthesis validated for clinical use. J. Label. Compd. Radiopharm. 56, 595–599.

Horti, A.G., Villemagne, V.L., 2006. The quest for Eldorado: development of radioligands for in vivo imaging of nicotinic acetylcholine receptors in human brain. Curr. Pharm. Des. 12, 3877–3900.

Horti, A.G., Scheffel, U., Koren, A.O., Ravert, H.T., Mathews, W.B., Musachio, J.L., Finley, P.A., London, E.D., Dannals, R.F., 1998. 2-[^{18}F]Fluoro-A-85380, an in vivo tracer for the nicotinic acetylcholine receptors. Nucl. Med. Biol. 25, 599–603.

Horti, A.G., Gao, Y., Kuwabara, H., Dannals, R.F., 2010. Development of radioligands with optimized imaging properties for quantification of nicotinic acetylcholine receptors by positron emission tomography. Life Sci. 86, 575–584.

Horti, A.G., Kuwabara, H., Holt, D.P., Dannals, R.F., Wong, D.F., 2013. Recent PET radioligands with optimal brain kinetics for imaging nicotinic acetylcholine receptors. J. Label. Compd. Radiopharm. 56, 159–166.

Innis, R.B., Cunningham, V.J., Delforge, J., Fujita, M., Gjedde, A., Gunn, R.N., Holden, J., Houle, S., Huang, S.C., Ichise, M., Iida, H., Ito, H., Kimura, Y., Koeppe, R.A., Knudsen, G.M., Knuuti, J., Lammertsma, A.A., Laruelle, M., Logan, J., Maguire, R.P., Mintun, M.A., Morris, E.D., Parsey, R., Price, J.C., Slifstein, M., Sossi, V., Suhara, T., Votaw, J.R., Wong, D.F., Carson, R.E., 2007. Consensus nomenclature for in vivo imaging of reversibly binding radioligands. J. Cereb. Blood Flow Metab. 27, 1533–1539.

Kas, A., Bottlaender, M., Gallezot, J.D., Vidailhet, M., Villafane, G., Grégoire, M.C., Coulon, C., Valette, H., Dollé, F., Ribeiro, M.J., Hantraye, P., Remy, P., 2009. Decrease of nicotinic receptors in the nigrostriatal system in Parkinson's disease. J. Cereb. Blood Flow Metab. 29, 1601–1608.

Kendziorra, K., Wolf, H., Meyer, P.M., Barthel, H., Hesse, S., Becker, G.A., Luthardt, J., Schildan, A., Patt, M., Sorger, D., Seese, A., Gertz, H.J., Sabri, O., 2011. Decreased cerebral α4β2* nicotinic acetylcholine receptor availability in patients with mild cognitive impairment and Alzheimer's disease assessed with positron emission tomography. Eur. J. Nucl. Med. Mol. Imaging 38, 515–525.

Kimes, A.S., Horti, A.G., London, E.D., Chefer, S.I., Contoreggi, C., Ernst, M., Friello, P., Koren, A.O., Kurian, V., Matochik, J.A., Pavlova, O., Vaupel, D.B., Mukhin, A.G., 2003. 2-[^{18}F]F-A-85380: PET imaging of brain nicotinic acetylcholine receptors and whole body distribution in humans. FASEB J. 17, 1331–1333.

Kuwabara, H., Wong, D.F., Gao, Y., Valentine, H., Holt, D.P., Ravert, H.T., Dannals, R.F., Horti, A.G., 2012. PET imaging of nicotinic acetylcholine receptors in baboons with ^{18}F-AZAN, a radioligand with improved brain kinetics. J. Nucl. Med. 53, 121–129.

Logan, J., Fowler, J.S., Volkow, N.D., Wolf, A.P., Dewey, S.L., Schlyer, D.J., MacGregor, R.R., Hitzemann, R., Bendriem, B., Gatley, S.J., Christman, D.R., 1990. Graphical analysis of reversible radioligand binding from time–activity measurements applied to [N-11C-methyl]-(−)-cocaine PET studies in human subjects. J. Cereb. Blood Flow Metab. 10, 740–747.

Mamede, M., Ishizu, K., Ueda, M., Mukai, T., Iida, Y., Fukuyama, H., Saga, T., Saji, H., 2004. Quantification of human nicotinic acetylcholine receptors with ^{123}I-5IA SPECT. J. Nucl. Med. 45, 1458–1470.

Marutle, A., Warpman, U., Bogdanovic, N., Nordberg, A., 1998. Regional distribution of subtypes of nicotinic receptors in human brain and effect of aging studied by (±)-[^{3}H]epibatidine. Brain Res. 801, 143–149.

Meyer, P.M., Strecker, K., Kendziorra, K., Becker, G., Hesse, S., Woelpl, D., Hensel, A., Patt, M., Sorger, D., Wegner, F., Lobsien, D., Barthel, H., Brust, P., Gertz, H.J., Sabri, O., Schwarz, J., 2009. Reduced alpha4beta2*-nicotinic acetylcholine receptor binding and its relationship to mild cognitive and depressive symptoms in Parkinson disease. Arch. Gen. Psychiatry 66, 866–877.

Mihailescu, S., Drucker-Colín, R., 2000. Nicotine, brain nicotinic receptors, and neuropsychiatric disorders. Arch. Med. Res. 31, 131–144.

Mo, Y.-X., Yin, Y.-F., Li, Y.-M., 2014. Neural nAChRs PET imaging probes. Nucl. Med. Commun. 35, 135–143.

Mukhin, A.G., Kimes, A.S., Chefer, S.I., Matochik, J.A., Contoreggi, C.S., Horti, A.G., Vaupel, D.B., Pavlova, O., Stein, E.A., 2008. Greater nicotinic acetylcholine receptor density in smokers than in nonsmokers: a PET study with 2-^{18}F-FA-85380. J. Nucl. Med. 49, 1628–1635.

O'Brien, J.T., Colloby, S.J., Pakrasi, S., Perry, E.K., Pimlott, S.L., Wyper, D.J., McKeith, I.G., Williams, E.D., 2007. Alpha4beta2 nicotinic receptor status in Alzheimer's disease using ^{123}I-5IA-85380 single-photon-emission computed tomography. J. Neurol. Neurosurg. Psychiatry 78, 356–362.

Okada, H., Ouchi, Y., Ogawa, M., Futatsubashi, M., Saito, Y., Yoshikawa, E., Terada, T., Oboshi, Y., Tsukada, H., Ueki, T., Watanabe, M., Yamashita, T., Magata, Y., 2013. Alterations in α4β2 nicotinic receptors in cognitive decline in Alzheimer's aetiopathology. Brain 136, 3004–3017.

Paterson, D., Nordberg, A., 2000. Neuronal nicotinic receptors in the human brain. Prog. Neurobiol. 61, 75–111.

Patt, J.T., Deuther-Conrad, W., Wohlfarth, K., Feuerbach, D., Brust, P., Steinbach, J., 2003. Norchloro-fluoro-homoepibatidine: ^{18}F-labelling and evaluation of affinity and selectivity at neuronal nicotinic acetylcholine receptors. J. Label. Compd. Radiopharm. 46 (S1), 168.

Patt, M., Schildan, A., Habermann, B., Fischer, S., Hiller, A., Deuther-Conrad, W., Wilke, S., Smits, R., Hoepping, A., Wagenknecht, G., Steinbach, J., Brust, P., Sabri, O., 2013. Fully automated radiosynthesis of both enantiomers of [^{18}F]Flubatine under GMP conditions for human application. Appl. Radiat. Isot. 80, 7–11.

Patt, M., Becker, G.A., Grossmann, U., Habermann, B., Schildan, A., Wilke, S., Deuther-Conrad, W., Graef, S., Fischer, S., Smits, R., Hoepping, A., Wagenknecht, G., Steinbach, J., Gertz, H.J., Hesse, S., Schönknecht, P., Brust, P., Sabri, O., 2014. Evaluation of metabolism, plasma protein binding and other biological parameters after administration of (−)-[^{18}F]Flubatine in humans. Nucl. Med. Biol. 41, 489–494.

Perry, E.K., Morris, C.M., Court, J.A., Cheng, A., Fairbairn, A.F., McKeith, I.G., Irving, D., Brown, A., Perry, R.H., 1995. Alteration in nicotine binding sites in Parkinson's disease, Lewy body dementia and Alzheimer's disease: possible index of early neuropathology. Neuroscience 64, 385–395.

Picard, F., Bruel, D., Servent, D., Saba, W., Fruchart-Gaillard, C., Schöllhorn-Peyronneau, M.A., Roumenov, D., Brodtkorb, E., Zuberi, S., Gambardella, A., Steinborn, B., Hufnagel, A., Valette, H., Bottlaender, M., 2006. Alteration of the in vivo nicotinic receptor density in ADNFLE patients: a PET study. Brain 129, 2047–2060.

Rinne, J.O., Myllykylä, T., Lönnberg, P., Marjamäki, P., 1991. A postmortem study of brain nicotinic receptors in Parkinson's and Alzheimer's disease. Brain Res. 547, 167–170.

Sabri, O., Kendziorra, K., Wolf, H., Gertz, H.J., Brust, P., 2008. Acetylcholine receptors in dementia and mild cognitive impairment. Eur. J. Nucl. Med. Mol. Imaging 35 (Suppl. 1), S30–S45.

Sabri, O., Wilke, S., Graef, S., Becker, G., Hesse, S., Sattler, B., Schoenknecht, P., Wagenknecht, G., Smits, R., Hoepping, A., Steinbach, J., Brust, P., 2012. PET imaging of cerebral nicotinic acetylcholine receptors (nAChRs) in early Alzheimer's disease (AD) assessed with the new radioligand (−)-[F-18]-norchloro-fluoro-homoepibatidine ([F-18]Flubatine). J. Cereb. Blood Flow Metab. 32, S55.

Saricicek, A., Esterlis, I., Maloney, K.H., Mineur, Y.S., Ruf, B.M., Muralidharan, A., Chen, J.I., Cosgrove, K.P., Kerestes, R., Ghose, S., Tamminga, C.A., Pittman, B., Bois, F., Tamagnan, G., Seibyl, J., Picciotto, M.R., Staley, J.K., Bhagwagar, Z., 2012. Persistent β2*-nicotinic acetylcholinergic receptor dysfunction in major depressive disorder. Am. J. Psychiatry 169, 851–859.

Sattler, B., Kranz, M., Starke, A., Wilke, S., Donat, C.K., Deuther-Conrad, W., Patt, M., Schildan, A., Patt, J., Smits, R., Hoepping, A., Schoenknecht, P., Steinbach, J., Brust, P., Sabri, O., 2014. Internal dose assessment of (−)-^{18}F-flubatine, comparing animal model data sets of mice and piglets with first-in-man results. J. Nucl. Med. 55, 1885–1892.

Scheffel, U., Horti, A.G., Koren, A.O., Ravert, H.T., Banta, J.P., Finley, P.A., London, E.D., Dannals, R.F., 2000. 6-[^{18}F]Fluoro-A-85380: an in vivo tracer for the nicotinic acetylcholine receptor. Nucl. Med. Biol. 27, 51–56.

Schildan, A., Patt, M., Sabri, O., 2007. Synthesis procedure for routine production of 2-[^{18}F]fluoro-3-(2(S)-azetidinylmethoxy)pyridine (2-[^{18}F]F-A-85380). Appl. Radiat. Isot. 65, 1244–1248.

Smits, R., Fischer, S., Hiller, A., Deuther-Conrad, W., Wenzel, B., Patt, M., Cumming, P., Steinbach, J., Sabri, O., Brust, P., Hoepping, A., 2014. Synthesis and biological evaluation of both enantiomers of [(18)F]flubatine, promising radiotracers with fast kinetics for the imaging of α4β2-nicotinic acetylcholine receptors. Bioorg. Med. Chem. 22, 804–812.

Sorger, D., Becker, G.A., Hauber, K., Schildan, A., Patt, M., Birkenmeier, G., Otto, A., Meyer, P., Kluge, M., Schliebs, R., Sabri, O., 2006. Binding properties of the cerebral alpha4beta2 nicotinic acetylcholine receptor ligand 2-[^{18}F]fluoro-A-85380 to plasma proteins. Nucl. Med. Biol. 33, 899–906.

Staley, J.K., Krishnan-Sarin, S., Cosgrove, K.P., Krantzler, E., Frohlich, E., Perry, E., Dubin, J.A., Estok, K., Brenner, E., Baldwin, R.M., Tamagnan, G.D., Seibyl, J.P., Jatlow, P., Picciotto, M.R., London, E.D., O'Malley, S., van Dyck, C.H., 2006. Human tobacco smokers in early abstinence have higher levels of beta2* nicotinic acetylcholine receptors than nonsmokers. J. Neurosci. 26, 8707–8714.

Turkheimer, F.E., Hinz, R., Cunningham, V.J., 2003. On the undecidability among kinetic models: from model selection to model averaging. J. Cereb. Blood Flow Metab. 23, 490–498.

Wong, D.F., Kuwabara, H., Kim, J., Brasic, J.R., Chamroonrat, W., Gao, Y., Valentine, H., Willis, W., Mathur, A., McCaul, M.E., Wand, G., Gean, E.G., Dannals, R.F., Horti, A.G., 2013. PET imaging of high-affinity α4β2 nicotinic acetylcholine receptors in humans with ^{18}F-AZAN, a radioligand with optimal brain kinetics. J. Nucl. Med. 54, 1308–1314.